

# Complex networks reveal early MRI markers of Parkinson's disease

Nicola Amoroso<sup>a,b</sup>, Marianna La Rocca<sup>a,b,\*</sup>, Alfonso Monaco<sup>b</sup>, Sabina Tangaro<sup>b</sup>, Roberto Bellotti<sup>a,b</sup>

<sup>a</sup>*Dipartimento Interateneo di Fisica "M. Merlin", Università degli studi di Bari "A. Moro", Italy*

<sup>b</sup>*Istituto Nazionale di Fisica Nucleare, Sezione di Bari, Italy*

---

## Abstract

Parkinson's disease (PD) is the most common neurological disorder, after Alzheimer's disease, and is characterized by a long prodromal stage lasting up to 20 years. As age is a prominent factor risk for the disease, next years will see a continuous increment of PD patients, making urgent the development of efficient strategies for early diagnosis and treatments. We propose here a novel approach based on complex networks for accurate early diagnoses using magnetic resonance imaging (MRI) data; our approach also allows us to investigate which are the brain regions mostly affected by the disease. First of all, we define a network model of brain regions and associate to each region proper connectivity measures. Thus, each brain is represented through a feature vector encoding the local relationships brain regions interweave. Then, Random Forests are used for feature selection and learning a compact representation. Finally, we use a Support Vector Machine to combine complex network features with clinical scores typical of PD prodromal phase and provide a diagnostic index. We evaluated the classification performance on the Parkinson's Progression Markers Initiative (PPMI) database, including a mixed cohort of 169 normal controls (NC) and 374 PD patients. Our model compares favorably with existing state-of-the-art MRI approaches. Besides, as a difference with previous approaches, our methodology ranks the brain regions according to disease effects without any *a priori* assumption.

*Keywords:* Parkinson's disease, MRI, Complex Networks, Machine learning

---

\*[marianna.larocca@ba.infn.it](mailto:marianna.larocca@ba.infn.it) (Marianna La Rocca)

*Email address:* [nicola.amoroso@ba.infn.it](mailto:nicola.amoroso@ba.infn.it) (Nicola Amoroso)

---

## 1. Introduction

Parkinson’s disease (PD) is a heterogeneous progressive neurological disorder, firstly described almost two centuries ago, basically related with early death of dopaminergic neurons in the substantia nigra and characterized by both motor and non-motor features (Gibb and Lees, 1988; Jankovic, 2008). It is recognized that age is the greatest risk factor for PD, its incidence reaches a maximum at about 80 years of age, thus the rising life expectancy is expected to increase the number of patients at more than 30% by 2030 (Dorsey et al., 2007).

The slow progression is one of the most important features of PD. The disease course can be roughly separated in two phases; the first prodromal, usually named “premotor”, phase can last up to 20 years and accounts for symptoms such as: impaired olfaction, constipation, depression, rapid eye movement sleep behavior disorder (RBD) and excessive daytime sleepiness (EDS) (Singaram et al., 1995; Gagnon et al., 2002; Chaudhuri et al., 2006). In fact, these symptoms could double the individual’s risk of developing the disease.

The second phase is early characterized by insurgence of typical bradykinesia, tremor and fatigue; then in the advanced stages by psychosis, dysphagia, freezing of gait, falls and postural instability (Friedman and Friedman, 1993; Huber et al., 1986). It is known that the average latency between the onset of prodromal and motor symptoms is about 12 – 14 years (Postuma et al., 2012). Thus, it would be of paramount importance the development of diagnostic strategies able to detect the disease in its prodromal phase and outline efficient markers. As shown in (Kalia and Lang, 2015), a prominent role in early diagnosis should be played by RBD, EDS, Hyposmia, depression and mild cognitive impairment (MCI) which are typical of the non-motor, prodromal or very early, PD phase, see Figure 1.

For what concerns imaging, candidate markers include positron emission tomography (PET) (Antonini et al., 1997; Hansen et al., 2016; Masdeu, 2017) or single photon emission computed tomography (SPECT) (Hirschauer et al., 2015; Suwijn et al., 2015; Adeli et al., 2017) methods. In fact, these methodologies can accurately detect PD. However, these methodologies are based on the detection of substantial losses of dopaminergic neurons, for example in the substantia nigra, whilst it would be desirable to diagnose the disease

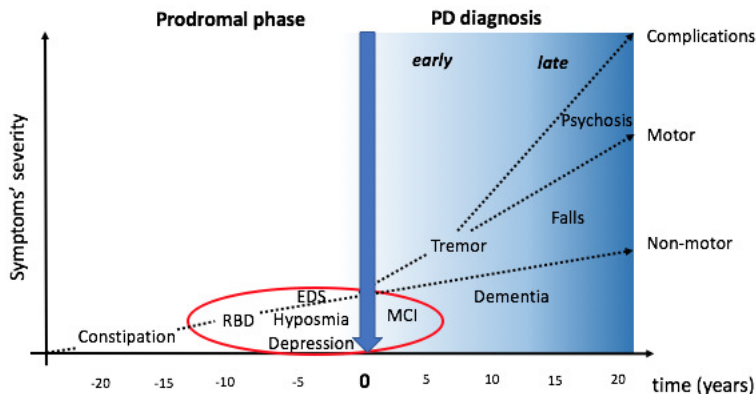


Figure 1: PD diagnosis is related to the onset of motor symptoms (time 0). The symptoms characterizing the prodromal phase and the years immediately following the diagnosis are: Rapid eye movement sleep Behavior Disorder (RBD), Excessive Daytime Sleepiness (EDS), Hyposmia (a reduced ability to smell and to detect odors) and mild cognitive impairment (MCI). Accordingly, these symptoms are usually enclosed in models trying to forecast the disease onset.

36 before this degeneration has occurred in order to enable early diagnosis be-  
 37 fore the onset of motor symptoms. With this regard, it should be taken into  
 38 account that PD patients could lose up to 80% of dopamine before symptoms  
 39 appear (Miller and O’Callaghan, 2015).

40 With this regard, the definition of new markers will play a fundamen-  
 41 tal role. It is clear that a single marker will not be able to allow accurate  
 42 diagnosis and monitor disease progression. Instead, a combination of dif-  
 43 ferent markers should provide a more reasonable approach. As previously  
 44 mentioned, PET and SPECT measures are very effective in the motor phase,  
 45 and they may support the diagnosis as well as monitor disease severity and  
 46 progression. Transcranial sonography is another promising approach whose  
 47 clinical applicability is still controversial (Bouwman et al., 2013; Pilotto  
 48 et al., 2015).

49 MRI markers could monitor structural changes in the brain and suggest  
 50 increased risk for PD (Salvatore et al., 2014) or be employed for differential  
 51 diagnosis of PD syndromes (Duchesne et al., 2009; Marquand et al., 2013;  
 52 Chagas et al., 2017). For example, voxel based morphometry (VBM) has  
 53 revealed significant gray matter reductions in PD patients with dementia  
 54 (Summerfield et al., 2005); MRI has also shown progressive atrophy in PD,  
 55 an effect already detectable in the early stage of the disease (Beyer et al.,

56 2007; Tessa et al., 2014). Thus, it would seem that there is still room to  
57 define effective MRI markers which outline the disease process before the  
58 death of dopaminergic neurons has triggered irreversible damages.

59 Several works have investigated the applicability of machine learning  
60 strategies to MRI data with fluctuating outcomes. (Focke et al., 2011) tried  
61 without success to use VBM features for individual classification using a Sup-  
62 port Vector Machine (SVM). However, (Cherubini et al., 2014) demonstrated  
63 that VBM features combined with diffusion tensor imaging can effectively  
64 distinguish PD patients from subjects with progressive supranuclear palsy.  
65 More recently, a synergistic paradigm combining Kohonen self organizing  
66 map and SVM claimed that MRI features can reach accurate classification  
67 performances including subjects with no dopaminergic deficit (Singh and  
68 Samavedham, 2015). Feature selection strategies seem to play a relevant role  
69 to define imaging markers accurately distinguishing PD patients from con-  
70 trols (Adeli et al., 2016). These different approaches share a not negligible  
71 feature, all of them rely on the supervised selection of PD-related regions of  
72 interest to obtain statistically significant associations between anatomy and  
73 clinical phenotype. Although these approaches reach excellent results, they  
74 can be limiting as they prevent the investigation of novel brain regions.

75 In this paper, we use MRI data from the Parkinson’s Progression Markers  
76 Initiative (PPMI) to extract imaging markers and learn an accurate classifi-  
77 cation model. With this goal, we introduce a brain connectivity model basing  
78 on gray matter and white matter voxel distribution. The proposed approach  
79 adopts a brain patch segmentation, thus it avoids common drawbacks of  
80 voxel-wise approaches, e.g. the lack of significance due to high dimensionality  
81 of the feature space. Besides, this methodology does not depend on fully-  
82 automated brain segmentation algorithms, whose accuracy could be poor,  
83 for region of interest definition. We measure how different brain regions are  
84 correlated and for each region we measure simple topological quantities; ac-  
85 cordingly, we build a model including atrophy effects locally induced by the  
86 disease and accounting for whole-brain modifications thanks to the network  
87 framework.

88 Complex network approaches have already proven their effectiveness in  
89 several cases, also in neuroimaging applications. MRI provides a useful base  
90 of knowledge when considering the topological organization of the brain.  
91 In fact, findings from structural (without excluding the functional) graphs  
92 point to a loss of highly connected areas in several brain diseases (Tijms  
93 et al., 2013). Graph theory provides two important methodological insights.

94 Firstly, it associates to each node quantitative measurements characterizing  
95 its role and importance within the network; secondly, it enables a direct  
96 description of the whole brain from a global perspective, thus letting emerge  
97 properties which affect the brain as a system (Bullmore and Sporns, 2009).

98 Several examples can be found for Alzheimer’s disease. (Stam et al.,  
99 2007) investigated small-worldness properties and found that diseased brains  
100 show a loss of connectivity. Also, the topological organization of the brain  
101 itself could be used as a marker; in fact, an increment of the shortest path  
102 length could denote an impaired organization (Lo et al., 2010). Another  
103 approach to detect the impairment of connectivity consists in measuring  
104 node-related quantities, as for example the rich-club property (Daianu et al.,  
105 2014). Finally, in previous works (La Rocca et al., 2017; Amoroso et al.,  
106 2017), we showed how complex network measures can be used to character-  
107 ize Alzheimer’s disease. Of course, PD has its specificities, for example it  
108 cannot be considered a disconnectivity disease. However, as previously men-  
109 tioned structural changes could be useful markers. It would be interesting  
110 to evaluate whether PD patients show significant brain structural changes,  
111 both locally and globally, and whether complex network measures can cap-  
112 ture these effects. In this work, basing on our previously mentioned works, we  
113 introduced a novel machine learning approach to combine network and clin-  
114 ical features within a unique classification score. Besides, we demonstrated  
115 its effectiveness on PD; as a matter of fact, we could not find any PD study  
116 investigating the adoption of complex network measures.

117 This work offers three main contributions: (i) we propose an unsupervised  
118 general methodology to model brain connectivity for both healthy subjects  
119 and patients; (ii) we explore which regions are significantly affected by the  
120 disease; (iii) we propose a novel learning strategy to combine network and  
121 clinical features; (iv) we define an accurate diagnostic tool for PD diagnosis  
122 basing only on MRI features; (v) we highlight the existence of an optimal  
123 scale to study PD. It is worth mentioning that previous approaches exploited  
124 *a priori* definition of regions of interest within the brain and therefore they  
125 could suffer a loss of information. In brief, the proposed approach can learn  
126 an accurate model to discriminate controls and patients and, eventually, de-  
127 tects possible novel imaging markers of the disease. Therefore, the use of  
128 MRI features becomes strategic for the development of early diagnosis tools  
129 or a better characterization of PD in its early stages.

130 **2. Materials**

131 Data used in preparation of this work was obtained from the Parkinson’s  
132 progression markers initiative (PPMI) database<sup>1</sup> (Marek et al., 2011). MRI  
133 data acquired by the PPMI for this study consisted of MPRAGE T1 brain  
134 scans from 3T SIEMENS MAGNETOM Trio scanners. Images were acquired  
135 with the following parameters: repetition time 2300 ms, echo time 2.98 ms,  
136 flip angle 9° and voxel size  $1 \times 1 \times 1 \text{ mm}^3$ , so that the equivalence 1 voxel =  
137  $1 \text{ mm}^3$  holds.

138 The PPMI is a clinical study whose main goal is the identification of PD  
139 markers in order to enhance the comprehension of the disease and eventually  
140 help the development of disease modifying therapies. The PPMI includes a  
141 mixed cohort of normal controls (NC) and PD patients; the database also  
142 includes subjects without dopaminergic deficits, namely SWEDD, that are  
143 disregarded in this work. Data from PPMI comes from different worldwide  
144 sites, along with structural MRI it is possible to find other imaging modalities  
145 such as SPECT or demographic and clinical metadata, such as age, gender  
146 and cognitive scores. NC subjects are both age- and gender-matched with  
147 the PD patients. It is worth noting that PD patients are *de novo* patients in  
148 that they are unmedicated, an important aspect as PD therapies could not  
149 have the desired effect of modifying the possible markers. More importantly,  
150 PD patients enrolled are mostly at the first stages of the disease, according to  
151 the Hoehn and Yahr scale (Hoehn et al., 1998); in fact, (Marek et al., 2011)  
152 explains that 98% of the subjects affected by the disease is in stages 1 and 2  
153 (over 5), corresponding to mild inconvenient without disabling symptoms.

154 The database consisted of two populations including respectively 107 male  
155 and 62 female NC, for a total of 169 subjects, and 243 male and 131 female  
156 patients, for an overall amount of 374 PD subjects. The populations are  
157 matched for age ( $60.2 \pm 11.5$  for NC and  $61.6 \pm 9.8$  for PD). In the fol-  
158 lowing Table 1 the baseline values for the Epworth Sleepiness Scale (ESS),  
159 the Geriatric Depression Scale (GDS), the Montreal Cognitive Assessment  
160 (MoCA), the Movement Disorder Society Unified Parkinson’s Disease Rating  
161 Scale (MDS-UPDRS) and the Rapid eye movement sleep Behavior Disorder  
162 (RBD) are enlisted.

163 ESS is a standardized simple measure for sleep propensity (Johns et al.,  
164 1991). Daytime sleepiness is usually associated to sleep disorders, but it can

---

<sup>1</sup><http://www.ppmi-info.org/data>.

Diagnosis	Age	ESS	GDS	MDS-UPDRS	MoCA	RBD
PD (374)	61.6 ± 9.8	3 [2, 6]	2 [1, 3]	29 [18, 41]	27 [26, 29]	5 [3, 8]
NC (169)	60.2 ± 11.5	2 [1, 4]**	1 [0, 2]**	27 [17, 37]*	28 [27, 29]**	5 [3, 8]

Table 1: Demographic and clinical information. Mean age and standard deviation are given, for other indicators with asymmetric distributions medians and interquartile ranges are preferred. Significant differences between normal controls (NC) and Parkinson’s disease (PD) are reported with the Kruskal-Wallis p-value (\* for  $p < 0.05$  and \*\* for  $p < 0.01$ ).

165 also be a symptom of prodromal PD phase along with RBD. Like constipation  
166 and olfactory disturbance, RBD can precede the development of the motor  
167 signs of Parkinson’s disease and longitudinal data suggest that RBD heralds  
168 the onset of motor symptoms in up to 40% of patients (Chaudhuri et al.,  
169 2006). RBD is measured according to the screening questionnaire proposed  
170 in (Stiasny-Kolster et al., 2007). ESS and RBD scores lie within ranges of  
171 normalcy for both NC and PD subjects, however PD patients showed a small  
172 but significant increment in ESS (Kruskal-Wallis p-value  $< 0.01$ ).

173 GDS score is based on a questionnaire of 30 items with binary outputs  
174 (Yesavage and Sheikh, 1986). For each affirmative answer 1 point is scored;  
175 healthy people should score  $5 \pm 4$ , mildly depressed and very depressed people  
176  $15 \pm 6$  and  $23 \pm 5$  respectively. In particular, for the present study, the shorter  
177 form was used (Yesavage et al., 2000). Accordingly, the subjects of the study  
178 were neither mildly nor very depressed, nevertheless PD patients showed a  
179 significantly higher GDS score (Kruskal-Wallis p-value  $< 0.01$ ).

180 The motor symptoms are taken into account by the Movement Disorder  
181 Society Unified Parkinson’s Disease Rating Scale (MDS-UPDRS) (Goetz  
182 et al., 2008). It is important to recall how the MDS-PD criteria assign a cen-  
183 tral role to motor symptoms to define clinical PD (Postuma et al., 2015); how-  
184 ever, also non-motor manifestations are present in many patients so that the  
185 related indicators can play a fundamental role for diagnosis, even though they  
186 cannot capture the complexity of this heterogeneous disease. As expected,  
187 MDS-UPDRS significantly distinguishes (Kruskal-Wallis p-value  $< 0.05$ ) the  
188 NC and PD cohorts.

189 Mild cognitive impairment (MCI) is a symptom commonly found in PD  
190 patients; it usually occurs with the onset of motor symptoms and may be a  
191 harbinger of dementia. MCI condition could be related to early PD symp-  
192 toms, such as RBD, in any case it is known that it may be found in up to  
193 80% of long term PD patients (Litvan et al., 2012). The Montreal Cognitive  
194 Assessment (MoCA) index is the preferred measure for accurate screening of

195 cognition in PD (Dalrymple-Alford et al., 2010). A final MoCA score of 26  
196 and above is considered normal: PD and NC cohorts of this study resulted  
197 normal on average with  $27.0 \pm 2.3$  and  $28 \pm 1$  respectively. A small but  
198 significant difference was observed (Kruskal-Wallis p-value  $< 0.01$ ).

### 199 3. Methods

200 The proposed approach aims at using MRI data to extract novel and effi-  
201 cient PD markers for early diagnosis. MRI scans from PPMI were processed  
202 to be both intensity and spatially normalized. Then, we introduced a con-  
203 nectivity model for each brain and obtained a feature representation using  
204 measures derived from the network description. Finally, we used the fea-  
205 ture representation to learn a supervised classification model within a **nested**  
206 cross-validation framework. Besides, as the NC and PD classes are not bal-  
207 anced, we performed a stratified cross-validation by granting for each round  
208 that the same number of subjects was sampled for the two classes. **The clas-**  
209 **sification consists of three distinct steps: firstly, Random Forest classifiers**  
210 **(Breiman, 2001) are used as a wrapper for feature selection; then, the im-**  
211 **portant features are used to feed, within the same cross-validation cycle, a**  
212 **second RF classifier in order to obtain a classification score for each subject;**  
213 **finally, an SVM classifier (Cortes and Vapnik, 1995) combines these scores**  
214 **and the other clinical features to discriminate the NC and PD classes. A**  
215 **schematic overview of the method is shown in the following Figure 2.**

216 The main goal of the method is to provide a classification score for PD.  
217 Besides, the methodology can be used to investigate which regions are mostly  
218 affected by the disease and rank them according to statistical significance.

#### 219 3.1. Image processing and network construction

220 MRI scans were skull stripped and aligned with an affine registration us-  
221 ing the FSL library developed by the Oxford Centre for Functional MRI of  
222 the Brain (FMRIB), specifically the Brain Extraction Tool (BET) (Smith,  
223 2002) and the FMRIB’s Linear Image Registration Tool (FLIRT) (Jenkinson  
224 and Smith, 2001; Jenkinson et al., 2002) were employed. Both the proce-  
225 dures were performed with default parameters, the reference image used for  
226 registration was the T1 MNI152 template with  $1 \times 1 \times 1$  mm<sup>3</sup> voxel size.  
227 Then, the scans were segmented in rectangular **non overlapping** boxes (from  
228 now onwards *patches*) of volume  $V = l_1 \times l_2 \times l_3$  using the medial longitu-  
229 dinal fissure to separate the left and right hemispheres. Accordingly, each



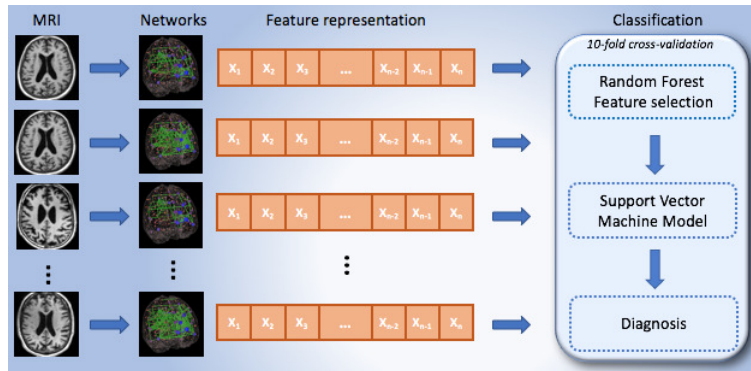


Figure 2: Methodology flowchart. MRI scans are processed to obtain a network representation, in particular they are preliminarily registered to the MNI152 brain template with an affine transformation. Then, for each node several features are computed and a feature representation is obtained. These features evaluate the node importance within the networks. The most informative features are selected with Random Forest wrapper and summarized in a classification score, then a Support Vector Machine combines these score with clinical features to distinguish NC and PD groups. The entire classification process is performed in 10-fold cross-validation.

230 hemisphere was divided in an equal number of patches. These patches were  
 231 considered the nodes of a weighted network having as weights the pairwise  
 232 Pearson’s correlation measured between each pair of nodes throughout the  
 233 whole brain.

234 The number of patches, a brain can be divided into, depends on the  
 235 volume  $V$ . As typical normalized volumes of substantia nigra range from 153  
 236 to 221  $\text{mm}^3$  (Kwon et al., 2012), we chose  $V = 125 \text{ mm}^3$  with  $l_1 = l_2 = l_3 = 5$   
 237 mm. Thus, the resulting networks consisted of 12219 nodes, each node of  
 238 the network consisting of a patch including 125 voxels. To evaluate the  
 239 presence of a link between two nodes we represented each patch through  
 240 a 125–dimensional vector and measured the pairwise Pearson’s correlation.  
 241 This measure emphasizes how similar two patches are, indeed, two patches  
 242 are highly correlated if, voxel by voxel, their gray levels are similar and  
 243 therefore if, spatially the distributions of white matter, gray matter and  
 244 cerebrospinal fluid (corresponding to voxel intensities of decreasing intensity)  
 245 are similar as well.

246 Correlations were measured in absolute value, thus disregarding left-right  
 247 symmetries, but keeping intact the informative content about structural mod-  
 248 ifications.

249 Thus, for each subject we introduced a complex network model. This  
250 model was investigated with measures borrowed by graph theory, particularly  
251 concerning weighted graphs. In order to remove noisy connections and avoid  
252 as far as possible the loss of strategical links, we thresholded the networks  
253 disregarding connections corresponding to less than moderate correlations  
254 ( $|r| < 0.3$ ). A study on how the threshold affects the capability of the  
255 network features to reveal pathological changes is reported in ??.

### 256 3.2. Feature representation

257 The underlying hypothesis of the proposed approach is that structural  
258 changes of the brain, measured by correlations, affect the connectivity pat-  
259 terns. We expect that these changes mostly concern (i) the intensity of the  
260 connections of a node, (ii) the number of connections a node has and (iii)  
261 which nodes it is connected with.

262 The first assumption holds because atrophic changes affecting a brain  
263 region tend to weaken the correlations of that specific region with other  
264 healthy GM/WM regions and enforce correlations with other atrophic regions  
265 or regions containing mostly CSF. As GM, WM and CSF are not evenly  
266 distributed, these changes should be detectable. The second assumption  
267 stands with the first one; as the intensity of connections changes, the number  
268 of connections must change too. Finally, the third assumption is a direct  
269 consequence of the first two: modifying the intensity of connections and the  
270 number of connections is equivalent to remove some links and create new  
271 ones. Accordingly, the organization itself of the networks should change;  
272 these effects can be detected with some specific complex network measures.

273 The intensity of connections of a network is, by definition, the strength  
274 of the network nodes. In order to detect how these structural changes of the  
275 brain are locally distributed, we considered the strength  $s_i$  of each node  $i$  of  
276 the network, *i. e.* the intensity of connections of a single patch.

277 Strength provides insight on the intensity of the connections of a partic-  
278 ular brain region, however without taking into account if the number of con-  
279 nectons is preserved. Of course, this second aspect should not be neglected,  
280 in fact it is in principle, possible, that a node  $i$  preserves its strength even  
281 losing or acquiring some connections, provided that the sum of the weights  
282 remains unchanged. Thus, to detect this effect, we measured, in addition  
283 to the strength, the inverse participation ratio  $Y_i^{-1}$  which evaluates how un-  
284 evenly the weights of the links of the node  $i$  are distributed (Menichetti et al.,  
285 2014):

$$Y_i = \sum_{j=1}^N \left( \frac{w_{ij}}{s_i} \right)^2. \quad (1)$$

286 to detect variations in brain connectivity among nodes with the same  
 287 degree  $k$ , which is the number of connections existing upon a node, we eval-  
 288 uated also the conditional values of strength  $s(k)$  and inverse participation  
 289 ratio  $Y^{-1}(k)$  for each subject and for each degree  $k$  ranging from 1 to 12219:

$$s(k) = \frac{1}{N_k} \sum_{i=1}^N s_i \delta(k_i, k); \quad (2)$$

$$Y(k) = \frac{1}{N_k} \sum_{i=1}^N Y_i \delta(k_i, k); \quad (3)$$

290 where  $N_k$  is node number having degree  $k$  and  $\delta$  is the Kronecker function  
 291 that is 1 when a node  $i$  has degree  $k$  and 0 otherwise. These measures  
 292 relate the intensity of the connections and their importance in the degree  
 293 distribution of the single subject networks. Finally, to better capture inter-  
 294 subject variations we considered the degree distribution of the whole training  
 295 cohort  $k^{global}$ , an array whose elements  $k_i^{global}$  indicate the number of links  
 296 connected to a node  $i$  over all the training subjects and we obtained the  
 297 previous 4 quantities  $s$   $Y^{-1}$   $s(k)$  and  $Y^{-1}(k)$  weighing them on the global  
 298 degree  $k^{global}$  and thus according to an overall perspective:

$$s'_i = \sum_{j=1}^N w_{ij} k_i^{global}; \quad (4)$$

$$Y'_i = \sum_{j=1}^N \left( \frac{w_{ij}}{s_i} \right)^2 k_i^{global}; \quad (5)$$

$$s'(k) = \frac{1}{N_k} \sum_{i=1}^N s'_i \delta(k_i, k); \quad (6)$$

$$Y'(k) = \frac{1}{N_k} \sum_{i=1}^N Y'_i \delta(k_i, k). \quad (7)$$

299 Thus, we obtained a 8-dimensional feature representation:  $s$ ,  $Y^{-1}$ ,  $s'$  and  
 300  $Y'^{-1}$  for each node and  $s(k)$ ,  $Y^{-1}(k)$ ,  $s'(k)$  and  $Y'^{-1}(k)$  for each degree.

301 *3.3. Feature selection and Classification*

302 Removing null mean and variance features and highly correlated features  
303 with a threshold of 0.7 from the feature representation obtained, 4048 fea-  
304 tures remain. For the feature reduction, we chose a moderate correlation  
305 threshold in order to reduce the great mole of features without losing in-  
306 formation. Using all the original features as input into Random Forest, be-  
307 sides being computationally intensive and time consuming, would not allow  
308 us to reduce high dimensionality of the model to increase its generalization  
309 and give a deep insight into underlying mechanisms. After the first feature  
310 reductions the still elevated dimensionality of the model required a higher  
311 feature selection level. There are three distinct approaches one could choose  
312 to tackle this task (Saeys et al., 2007): filter methods are fast and scalable,  
313 but they ignore possible interactions among the features; wrapper methods  
314 are computationally intensive in that they explore the space of features by  
315 evaluating random subsets and using supervised classifiers to find optimal  
316 configurations, but they are able to take into account feature interactions;  
317 embedded techniques are those for which the search for best discriminating  
318 features is built within the model.

319 We chose a hybrid approach in that we used Random Forests for feature  
320 selection but not for the model. Random Forests are an ensemble of clas-  
321 sification trees, whose trees are grown by bootstrapping training data and  
322 randomly selecting at each split a candidate set of features. Given  $f$  fea-  
323 tures, at each split  $\sqrt{f}$  features are randomly picked and each tree is grown  
324 unpruned to obtain low-bias models; the main idea behind Random Forests  
325 is the use of random variable selection resulting in low correlation of single  
326 trees; as a consequence, the overall classifier yields a model that can achieve  
327 both low bias and low variance (Breiman, 1996).

328 Random Forests are particularly suitable for the present analysis where  
329 the number of variables exceeds the observations (Díaz-Uriarte and De An-  
330 dres, 2006). Moreover, it is a robust and easy-to-tune model, it does not  
331 overfit thanks to internal bagging and, more importantly, it provides a con-  
332 tinuous measure of feature importance. For our experiments we used the  
333 implementation provided by *R version* 3.2.2 with the package *randomForest*  
334 *version* 4.6 – 10; a standard configuration was used: each forest was grown  
335 with 500 trees.

336 We adopted a hierarchical combination of two forests. For each 10-  
337 fold cross-validation round, the first forest, for each split, randomly picked  
338  $\sqrt{f} = \sqrt{4048}$  features and selected a number of features, which were on

339 average 60. Features found by the first classifier were chosen in order to  
340 exceed in importance the third quartile of importance distribution computed  
341 in terms of mean accuracy decrease. Then a second forest within the same  
342 cross-validation cycle, was trained with these selected features to obtain a  
343 classification score. The results of this procedure were twofold: on one hand  
344 we selected the most discriminative features and on the other hand we sum-  
345 marized the whole information content provided by the complex network  
346 measures in a unique score. Thus, this score outlined which subjects had  
347 shown brain structural and topological changes significantly associated to  
348 the diagnosis. The presence of brain regions with modified centrality, the  
349 disrupt of connectivity, along with the previously mentioned properties con-  
350 cerning for example the intensity or the uniformity of connections, were all  
351 included in the classification score.

352 We designed this approach as the number of features deriving from the  
353 complex network description can be overwhelming if compared to the avail-  
354 able clinical features of Table 1. It is important to remind that for each  
355 subject clinical features are provided at the baseline. Accordingly, a diag-  
356 nostic model relying on clinical features of prodromal or early PD phase and  
357 structural MRI data was designed. Finally, for the discrimination of PD pa-  
358 tients and normal controls, we trained a third radial Support Vector Machine  
359 (SVM) classifier combining the classification score and the clinical features  
360 and keeping fixed the training and validation set of the previous 10-fold cross-  
361 validation. For our analysis we used the *R* package *e1071 version 1.6-7* with  
362 the default implementation (cost = 1 and gamma = 0.003).

## 363 4. Results

### 364 4.1. Classification performance

365 The proposed methodology both detects which regions are mostly affected  
366 by the disease and uses the network measures to provide a classification score.  
367 Besides, the use of clinical features concerning the PD prodromal phase or  
368 the disease onset can support the early diagnosis. In order to evaluate the  
369 effectiveness of the proposed procedure we used standard machine learning  
370 techniques, such as the previously mentioned Random Forests and SVM algo-  
371 rithms. All the presented results were acquired with a 10-fold cross-validation  
372 framework. We measured the informative content provided by our complex  
373 network approach combined with the clinical features **training an SVM classi-**  
374 **fier**. Besides, we separately evaluated the informative content **of respectively**

375 the network measures, using the classification score of a Random Forest (RF)  
 376 classifier, and the clinical features, training an SVM classifier. The results  
 377 are shown in Figure 3.

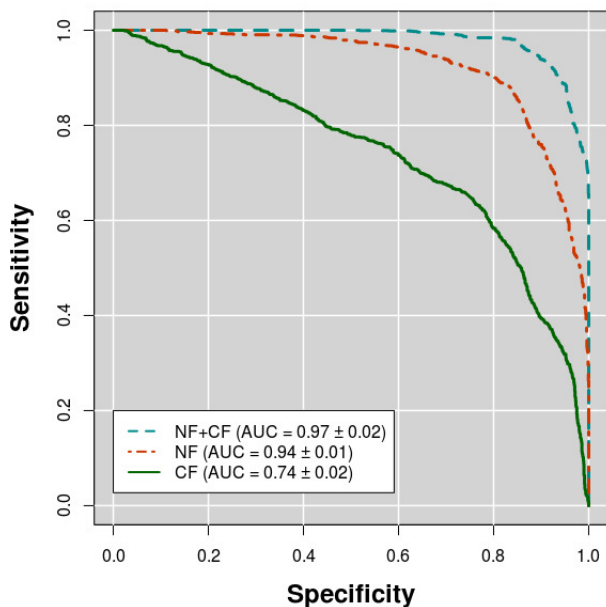


Figure 3: Classification performance in terms of area under the receiver operating characteristics curve (AUC). The combined use of network features (NF) and clinical features (CF) reaches the highest AUC =  $0.97 \pm 0.02$  (cyan dashed line). CF on their own reach an AUC =  $0.74 \pm 0.02$  (dark green continuous line), which is reasonable for baseline subjects whose symptoms are mild. NF provide effective markers for PD, in fact basing on these feature it is possible to diagnose PD with an AUC =  $0.94 \pm 0.01$  (dark red dash-dot line).

378 The combined use of MRI and clinical features gives the best performance  
 379 as summarized in Table 2.

380 Area under the receiver operating characteristics  $AUC = 0.97 \pm 0.02$ ,  
 381 accuracy  $ACC = 0.93 \pm 0.04$ , sensitivity  $sens = 0.92 \pm 0.06$  and specificity  
 382  $spec = 0.93 \pm 0.07$ . These results were significantly higher than those obtained  
 383 by using only the complex network measures; in fact, we found in this case  
 384  $AUC = 0.94 \pm 0.01$ ,  $ACC = 0.88 \pm 0.06$ ,  $sens = 0.85 \pm 0.09$  and  $spec =$   
 385  $0.88 \pm 0.09$ . These results were averaged on 1000 cross-validation rounds

features	AUC	ACC	sens	spec
Network measures	$0.94 \pm 0.01$	$0.88 \pm 0.06$	$0.85 \pm 0.09$	$0.88 \pm 0.09$
Clinical scores	$0.77 \pm 0.01$	$0.70 \pm 0.08$	$0.65 \pm 0.12$	$0.75 \pm 0.11$
Both	<b><math>0.97 \pm 0.02</math></b>	<b><math>0.93 \pm 0.04</math></b>	<b><math>0.93 \pm 0.06</math></b>	<b><math>0.92 \pm 0.07</math></b>

Table 2: NC vs PD classification performances for feature typology. Area under the receiver operating characteristics (AUC), accuracy (ACC), sensitivity (sens) and specificity (spec) are reported with the relative standard deviations. Best performance (bold) is obtained with a combined use of network and clinical features.

386 and significance was assessed with  $z$ -tests; for all comparisons we found 1%  
387 significance.

388 Clinical features resulted in a classification performance significantly lower  
389 than those previously reported. Thus, the information content provided by  
390 the proposed model gives a significant contribution. In particular, we found  
391 when using only the clinical features:  $AUC = 0.77 \pm 0.01$ ,  $ACC = 0.70 \pm 0.08$ ,  
392  $sens = 0.66 \pm 0.12$  and  $spec = 0.73 \pm 0.11$ . Figure 4 allows us to appreciate  
393 this effect from a different perspective.

394 Classification scores based only on clinical features consistently tend to  
395 overlap and assign to PD subjects low scores. In fact, sensitivity, which is ba-  
396 sically the discriminative power for positive subjects, is lower than specificity.  
397 On the contrary, the discrimination of the two classes is greatly enhanced  
398 when introducing complex network markers.

#### 399 4.2. Comparison with standard methods

400 In order to assess the effectiveness of the proposed approach, we com-  
401 pared its classification accuracy with that of two standard approaches. In  
402 particular, we used FreeSurfer Fischl (2012) to extract some structural fea-  
403 tures, such as grey matter and white matter volumes of subcortical brain  
404 structures or the average cortical thickness of specific regions for a total of  
405 181 ROI features. Then, we performed a standard VBM pipeline Ashburner  
406 and Friston (2000) to detect voxels showing a significant (p-value < 0.01)  
407 association with the diagnosis, these voxels provided another feature repre-  
408 sentation. Both, the ROI and the VBM descriptions were used to feed the  
409 classification framework previously described. In this way, we obtained a  
410 direct comparison evaluating the informative power of the proposed method-  
411 ology and ROI/VBM approaches, see Figure 5.

412 The proposed method ( $AUC = 0.97 \pm 0.02$ ) compares favorably with VBM  
413 ( $AUC = 0.93 \pm 0.04$ ) and ROI ( $AUC = 0.82 \pm 0.06$ ) descriptions. It is worth

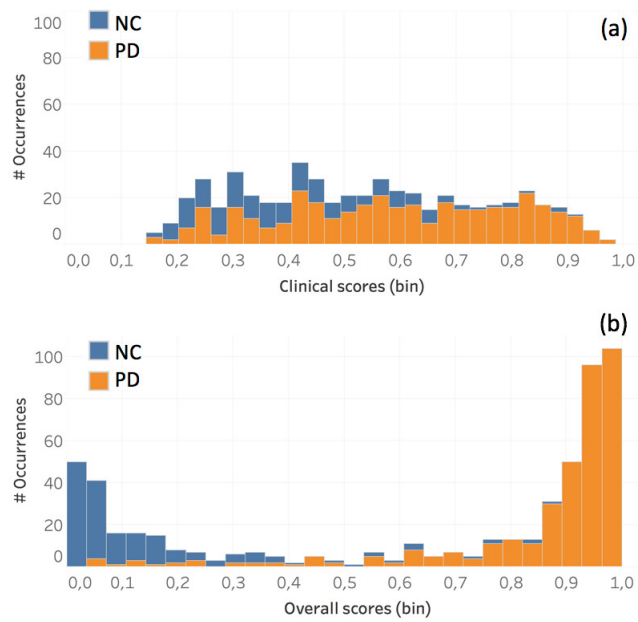


Figure 4: The classification score distribution using (a) only clinical features and (b) combining them with network measures. Each column of the histogram contains the number of NC subjects (blue) and PD patients (orange) whose score lies in that bin. Classification scores obtained using both network and clinical features show a greatly enhanced class separation.



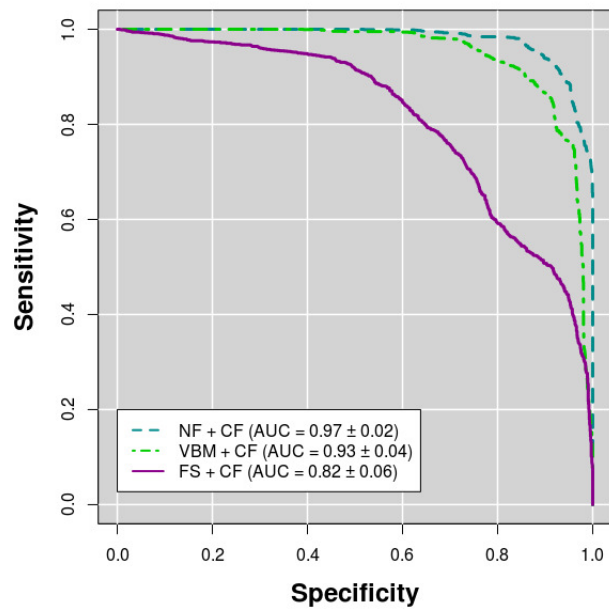


Figure 5: Classification performance in terms of area under the receiver operating characteristics curve (AUC). The combined use of network features (NF) and clinical features (CF) reaches the highest AUC =  $0.97 \pm 0.02$  (cyan dashed line). The combination of Voxel Based Morphometry (VBM) features and CF reaches an AUC =  $0.93 \pm 0.04$  (light green dash-dot line). Finally, FreeSurfer features (FS) combined to CF give an AUC =  $0.82 \pm 0.06$  (magenta continuous line).

414 mentioning that even when not considering clinical features, the network  
 415 description remains the most effective ( $AUC = 0.94 \pm 0.01$ ) both in respect  
 416 of VBM ( $AUC = 0.87 \pm 0.05$ ) and ROI ( $AUC = 0.70 \pm 0.06$ ) approach. A  
 417 summary of this comparison is presented in Table 3.

features	AUC	ACC	sens	spec
NF + CF features	<b><math>0.97 \pm 0.02</math></b>	<b><math>0.93 \pm 0.04</math></b>	<b><math>0.93 \pm 0.06</math></b>	<b><math>0.92 \pm 0.07</math></b>
VBM + CF	$0.93 \pm 0.04$	$0.86 \pm 0.06$	$0.88 \pm 0.08$	$0.86 \pm 0.08$
FS + CF	$0.82 \pm 0.06$	$0.72 \pm 0.07$	$0.74 \pm 0.10$	$0.71 \pm 0.12$
NF	$0.94 \pm 0.01$	$0.88 \pm 0.06$	$0.85 \pm 0.09$	$0.88 \pm 0.09$
VBM	$0.87 \pm 0.05$	$0.79 \pm 0.08$	$0.77 \pm 0.12$	$0.77 \pm 0.11$
FS	$0.70 \pm 0.06$	$0.63 \pm 0.07$	$0.60 \pm 0.11$	$0.66 \pm 0.11$

Table 3: NC vs PD classification performances for network features (NF), Voxel Based Morphometry (VBM) and FreeSurfer (FS) obtained with and without the combination of clinical features (CF). Area under the receiver operating characteristics (AUC), accuracy (ACC), sensitivity (sens) and specificity (spec) are reported with the relative standard deviations. Best performance (bold) is obtained with a combined use of network and clinical features (NF+CF). The combination with the clinical features improves the performances in all three cases (NF+CF,VBM+CF,FS+CF).

### 418 4.3. Regions of interest

419 The high discriminative power shown by the features and evaluated in the  
 420 previous section demonstrates the reliability of the complex network mea-  
 421 sures as PD markers. Besides the diagnostic support that these features can  
 422 provide, it is interesting to evaluate which regions result to be affected by the  
 423 disease and eventually rank them according to their statistical significance.

424 For each cross-validation round we recorded which features were selected  
 425 as the most important for classification and outlined the brain regions related  
 426 to them. Accordingly, for each cross-validation round we counted whether or  
 427 not a particular anatomic district had been selected and tested the hypothesis  
 428 that these occurrences had happened by chance. The null hypothesis is that  
 429 a region should be selected according to a Bernoulli distribution with an *a*  
 430 *priori* probability  $1/12219$ , which is the total number of patches. We tested  
 431 the occurrence of a specific region against the random occurrence rate which  
 432 was in our case equal to  $1/\text{patch number}$  ( $1/12219$ ), which is in conclusion  
 433 the number of the carried tests. Figure 6 shows some of the significant regions  
 434 associated to the diagnosis.

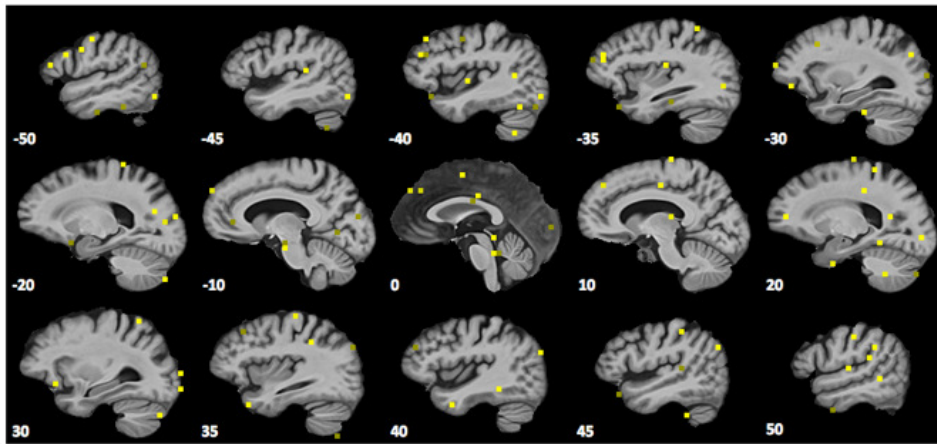


Figure 6: A qualitative overview of significant PD-related patches, as they are outlined by complex network measures, is represented along sagittal planes. More significant patches have a lighter shade of yellow and little by little less significant patches have a darker shade of yellow. The negative planes belong to the left hemisphere while the positive planes belong to the right one.

435 According to the proposed method, 186 significant patches were detected:  
 436 43% within the right hemisphere and 40% within the left one; 9% of patches  
 437 were located in the cerebellum; brainstem regions appeared in 3% of cases.  
 438 There is not a great difference between GM and WM regions, in fact the  
 439 GM regions selected are 53%, the WM ones 46%. The vast majority of  
 440 brain regions affected by PD lies in the Frontal (27%), Occipital (21%) and  
 441 Temporal (15%) lobes. For a complete overview of the selected regions and  
 442 the relative p-values please refer to the Appendix. Instead, we provide in the  
 443 following Table 4 a compact overview of the first 15 selected patches.

Region	p-value
(L) Temporal Lobe. Middle Temporal Gyrus. GM-WM. Ba 39.	$7.2 \cdot 10^{-7}$
(R) Temporal Lobe. Superior and Inferior Temporal Gyrus. GM-WM. Ba 22.	$7.2 \cdot 10^{-7}$
(R) Occipital Lobe. Sub-Gyral (WM).	$3.6 \cdot 10^{-6}$
(L) Occipital Lobe. Superior Occipital Gyrus GM-WM. Ba 19.	$4.6 \cdot 10^{-6}$
(R) Frontal Lobe. Middle Frontal Gyrus (WM).	$5.3 \cdot 10^{-6}$
(L-c) Anterior Lobe. Culmen (GM).	$5.9 \cdot 10^{-6}$
(R) Frontal Lobe. Medial Frontal Gyrus (WM).	$5.9 \cdot 10^{-6}$
(R) Frontal Lobe. Precentral Gyrus. GM. Ba 44.	$5.9 \cdot 10^{-6}$
(L) Limbic Lobe. Cingulate Gyrus. GM. Ba 24.	$5.9 \cdot 10^{-6}$
(R) Parietal Lobe. Precuneus (WM).	$5.9 \cdot 10^{-6}$
(L) Frontal Lobe. Middle Frontal Gyrus. GM. Ba 46.	$6.2 \cdot 10^{-6}$
(L) Brainstem. Midbrain	$6.6 \cdot 10^{-6}$
(L) Temporal Lobe. Fusiform Gyrus GM-WM. Ba 37.	$7.2 \cdot 10^{-6}$
(R-c) Posterior Lobe. Declive. GM.	$7.2 \cdot 10^{-6}$
(R) Temporal Lobe. Fusiform Gyrus. WM.	$7.2 \cdot 10^{-6}$

Table 4: The regions selected according to complex network measures and the inherent level of significance with respect of diagnosis. (L) and (R) denotes the left and right hemispheres; cerebellum regions are denoted with c. Brodmann areas (Ba) are also outlined when appropriate.

444 These regions have been already detected in several PD studies (Li et al.,  
 445 2017; Warmuth-Metz et al., 2001; Kim et al., 2013; Wen et al., 2015), an-  
 446 other indirect validation of the proposed methodology in that the selected  
 447 regions consistently correspond to regions whose relationship with the disease  
 448 is established.

#### 449 4.4. Robustness of the method

450 In this section we demonstrate that the proposed complex network de-  
 451 scription does not require any fine tuning, accordingly we used for both image  
 452 processing and classification standard configurations, then we evaluated, a

453 posteriori, that choosing other configurations would not have affected the  
 454 obtained results. We evaluated the relation between the threshold used to  
 455 remove some edges from the network and the classification accuracy; a wide  
 456 range of thresholds was explored, see Figure 7. Threshold was varied from  
 457 0 to 0.9 with 0.1 steps and with a fixed patch volume of 125 voxels. The  
 458 maximum value of the classification accuracy was obtained at 0.3 threshold.  
 459 It is worth noting that this value also corresponded to minimum variance.  
 460 Accuracy remained constant at 0.93 for a wide range of correlations [0.3, 0.5],  
 461 thus confirming that the method does not require a fine tuning of threshold  
 462 values. For higher threshold values, there was a significant performance drop,  
 463 suggesting that too high threshold values cause the loss of important links.

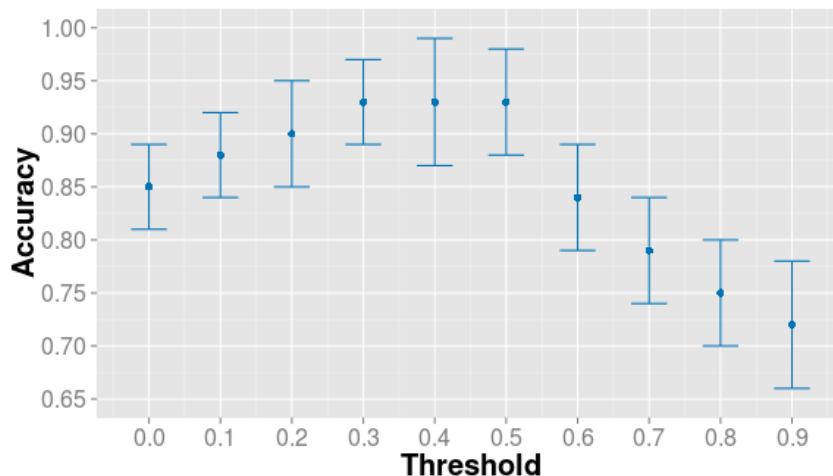


Figure 7: The figure shows the accuracy as a function of the threshold that changes from 0 to 0.9. In correspondence of a threshold value of 0.3, the best accuracy and the minimal standard deviation were reached.

464 As demonstrated in section 4.1, the proposed complex network approach  
 465 significantly enhances the discriminative power of clinical features. The  
 466 network measures derived from MRI data effectively characterize PD pat-  
 467 terns. To evaluate the robustness of the informative content provided by our  
 468 method, we explored the hyperparameter space. Firstly, we evaluated the  
 469 cost parameter which plays a fundamental role for Support Vector Machines,  
 470 see Figure 8.

471 In fact, the cost determines how much the SVM model should fit the  
 472 training data by varying the margins of the decision hyperplane, larger values

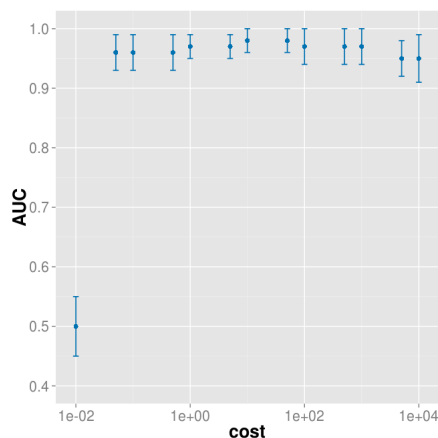


Figure 8: The classification performance in terms of AUC remains stable by varying the cost parameter. For tiny cost values the decision hyperplane margins are too large and the performance drops.

473 of cost correspond to smaller margins. The results show that for a wide range  
 474 of cost values the classification performance remains stable granting robust  
 475 results. When the cost reaches the 0.01 value the performance drops, this  
 476 means that the margins have become so large that the model cannot just fit  
 477 the data. Moreover, we investigated the model robustness with respect of  
 478 the gamma parameter which defines how far the region of influence of each  
 479 training example should extend, see Figure 9.

480 As gamma controls the variance of the model, by varying gamma one  
 481 can move from a high-bias to a high-variance model. Of course, the optimal  
 482 classification region stands between these two cases. The results show that for  
 483 the present model a wide stability region exists, in fact the AUC consistently  
 484 remains over the 0.90 value for a gamma variation of more than 4 orders of  
 485 magnitude.

#### 486 4.5. Evaluation of the informative content

487 To evaluate the goodness of complex network measures as PD markers  
 488 it is not sufficient to demonstrate that these features allow an accurate and  
 489 robust classification. First of all, looking at the classification performance it  
 490 is not possible to guess if credit should be given to the SVM classification  
 491 model or the informative content of the features. As such, we compared  
 492 the classification performance of several state-of-the-art classifiers, specifi-  
 493 cally we investigated Random Forest (RF), Naive Bayes (NB) and Neural

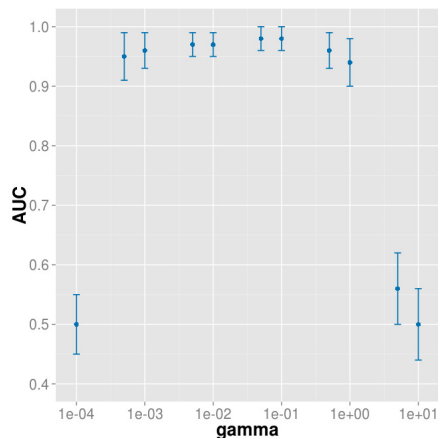


Figure 9: Varying the gamma parameter it is possible to switch from high-bias to high-variance models, in this case however the optimal classification region extends for more than 4 orders of magnitude.

494 Network (NN) classifiers. For each method we explored within a nested  
 495 cross-validation the hyperparameter space and several configurations, only  
 496 optimal configuration results are reported in the following Table 5.

method	AUC	ACC	sens	spec
Neural Network	0.94 ± 0.04	0.89 ± 0.05	0.90 ± 0.08	0.88 ± 0.07
Random Forest	0.97 ± 0.02	0.91 ± 0.05	0.90 ± 0.07	0.91 ± 0.07
Naive Bayes	0.97 ± 0.03	0.92 ± 0.05	0.91 ± 0.07	<b>0.93 ± 0.07</b>
Support Vector Machine	<b>0.97 ± 0.02</b>	<b>0.93 ± 0.04</b>	<b>0.93 ± 0.06</b>	0.92 ± 0.07

Table 5: A comparison between different machine learning methods (Neural Networks, Random Forests, Naive Bayes and Support Vector Machine classifiers) shows that the proposed complex network approach allows a robust diagnosis independently from the choice of the classifier, although Support Vector Machine reaches slightly better results (in bold) for almost each metric: area under the receiving operating characteristics (AUC), accuracy (ACC), sensitivity (sens) and specificity (spec).

497 The table shows that no significant difference can be found between dif-  
 498 ferent models, even if SVM would seem to perform slightly better than the  
 499 others. These results demonstrate that beyond the differences due to the ma-  
 500 chine learning models adopted, the proposed approach yields an outstanding  
 501 base of knowledge for PD discrimination.

502 However, this test does not evaluate the agreement between the models.  
 503 In fact, in principle two distinct models could perform equally but misclassi-

504 fying different subjects. In order to assess the agreement between our chosen  
 505 SVM model and the other models, we investigated the relationships existing  
 506 between the classification scores. The results are presented in Figure 10.

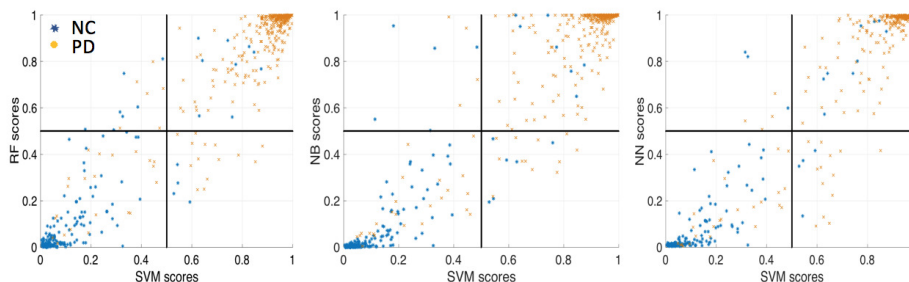


Figure 10: From left to right the agreement between the scores obtained with Support Vector Machine (SVM) and those obtained by: Random Forest (RF), Naive Bayes (NB) and Neural Network (NN) classifiers. The scores are densely distributed in top right and bottom left quadrants, where their predictions agree. Looking at the top left and bottom right quadrants it can be noted that, when in disagreement, SVM scores tend to be slightly more accurate than other scores.

507 The classification scores are densely distributed in the top right and bot-  
 508 tom left quadrants. The top right quadrant includes subjects whose classifi-  
 509 cation scores exceed the 0.5 value, it is the case of subjects diagnosed with  
 510 PD from both the SVM model, which is always reported on the  $x$  axis, and  
 511 the other models, which are reported instead on the  $y$  axis. Analogously,  
 512 the bottom left quadrant includes those subjects, whose classification scores  
 513 are lower than 0.5, for which the models agree assigning a NC status. As  
 514 expected from previous measures, the models correctly distinguish the two  
 515 classes, in fact in the top right quadrant the vast majority of subjects is  
 516 shown in orange, as subjects have mostly a PD diagnosis, and in the bottom  
 517 left the vast majority is in blue, as subjects are mainly NC.

518 The top left and bottom right quadrants are the regions of disagreement.  
 519 In these regions, in fact, the SVM model assigns a diagnosis different from  
 520 other models. For example, a subject belonging to the bottom right quadrant  
 521 has an SVM score  $> 0.5$  and it is accordingly diagnosed as PD but a RF  
 522 score (or NB/NN)  $< 0.5$  and it is therefore labeled as NC. First of all, it  
 523 is worth noting that these two quadrants are sparsely populated, especially  
 524 compared to the top right and bottom left ones, therefore this is a further  
 525 demonstration of the agreement between the models; besides, SVM tends to  
 526 be more accurate.



527 Keeping on with our example, in the bottom right quadrant for all the  
528 three cases the majority of subjects is orange, meaning that their true label  
529 is PD. This means that the SVM predictions is the right one. The same  
530 consideration holds for the top left quadrant, where the majority of subjects  
531 is represented in blue, and, again SVM correctly labels them as NC.

#### 532 4.6. Scale study and VBM

533 The proposed approach depends on the size of the brain patches used for  
534 the complex network model. In our previous studies concerning Alzheimer’s  
535 disease (La Rocca et al., 2017; Amoroso et al., 2017) we observed that one key  
536 aspect of complex network descriptions is that they let naturally emerge a  
537 dimensional scale, which is typical of the disease. For example, for Alzheimer  
538 characterization the best results were obtained with patches having approxi-  
539 mately a volume of 3000 mm<sup>3</sup>. Accordingly, in this work we explored a wide  
540 range of patch volumes and measured the [training](#) classification accuracy, see  
541 Figure 11.

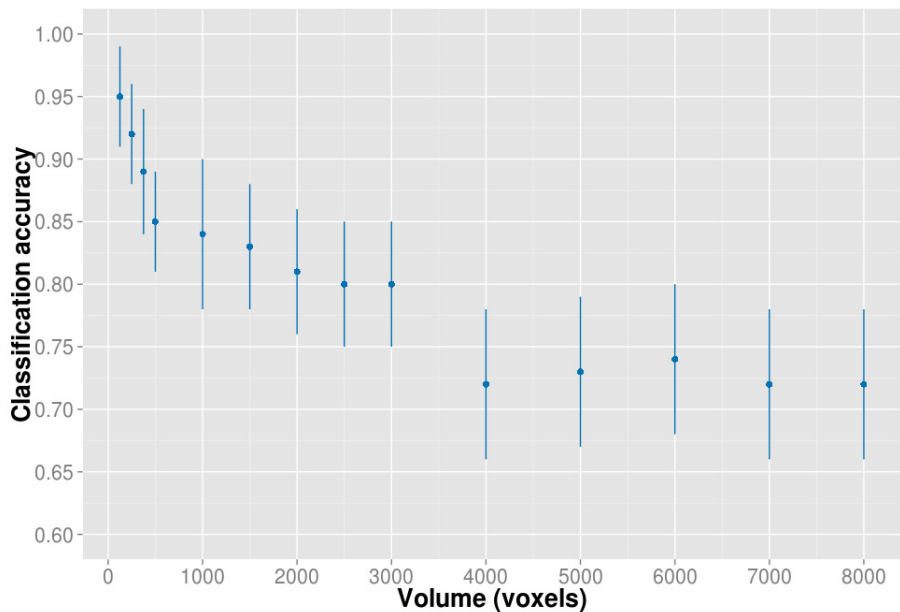


Figure 11: The optimal patch dimension expresses the existence of a preferred dimension or scale for PD markers. In particular, best classification accuracy  $0.95 \pm 0.04$  is obtained with smaller patches ( $5 \times 5 \times 5$  voxels). For larger patch dimensions the performance drops and reaches a stable plateau.

542 The classification accuracy decreases monotonically. The best perfor-  
543 mance was obtained with patches of  $5 \times 5 \times 5$  voxels. This result is sig-  
544 nificantly different from what we observed in Alzheimer. Moreover, when  
545 the patch volume reaches 4000 voxels (we remind here that for the present  
546 study voxels and  $\text{mm}^3$  can be interchangeably used) the accuracy remains  
547 constantly around 0.73.

548 We used a standard VBM pipeline to segment gray and white matter of  
549 each MRI scan. Then we normalized each subject to the MNI152 template  
550 and extracted the t-Student maps to determine if some clusters of voxels  
551 ( $> 30$ ) exhibit an association with the diagnosis. We found a good agree-  
552 ment with the regions detected with our complex network description, see  
553 Figure 12 for an overview, but, remarkably, the number of regions showing  
554 an association with the clinic was consistently reduced.

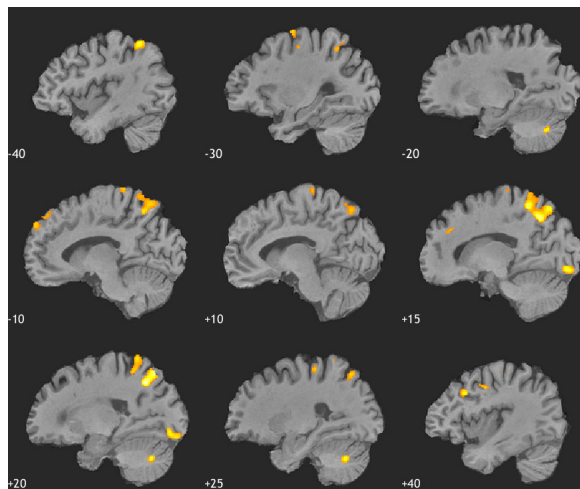


Figure 12: Voxel based morphometry shows the presence of some clusters (the sagittal plane is reported), however these regions represent only a subset of those outlined by our approach.

555 However, as explained in Section 1, voxel-wise approaches have an intrinsic  
556 drawback in that the need for thousands of multiple comparisons dramati-  
557 cally lowers the statistical power of commonly available datasets. Indeed,  
558 we found no significant association after Bonferroni corrections.

## 559 5. Discussion

560 The PD onset is characterized by clinical symptoms which emerge when  
561 the dopaminergic deficit has reached a considerable level. Therapies or drugs  
562 could easily be ineffective at this stage. This is why the identification of  
563 accurate markers, and hopefully of a diagnostic framework, based on symp-  
564 toms related to the prodromal or early phases of the disease is urgent. Our  
565 approach uses complex network measures to characterize PD patterns and  
566 develop a fully-automated machine learning diagnosis support system. The  
567 proposed methodology is robust and accurate. In addition, it provides de-  
568 tailed information about the brain regions mostly affected by the disease as  
569 it ranks them by associating an easy-to-interpret level of significance; thus,  
570 this method opens the possibility for further comprehension of PD patterns.

571 The proposed approach reaches an accurate diagnosis ( $AUC = 0.97 \pm 0.02$   
572 and  $ACC = 0.93 \pm 0.04$ ) and these results compare favorably with other  
573 state-of-the-art approaches. Among the most recent methodologies, the joint  
574 feature-sample selection algorithm by (Adeli et al., 2016) reports an 82% ac-  
575 curacy and currently achieves one of the best classification performances  
576 when using only MRI data. It is worth mentioning that other studies us-  
577 ing structural MRI features reported interesting results, such as (Salvatore  
578 et al., 2014) whose VBM-based methodology allowed an accuracy of 83.2%,  
579 although a significantly smaller sample including only 28 controls and 28 PD  
580 subjects.

581 It has been recently shown that accurate diagnosis (97.5%) can be ob-  
582 tained when combining both MRI and SPECT data (Adeli et al., 2017).  
583 However, such a study demonstrates that the classification accuracy almost  
584 relies on SPECT as SPECT provides a diagnostic accuracy of 95.6% when  
585 used without MRI. Thus, MRI data seems to slightly contribute to diagnosis  
586 accuracy. Nevertheless, as SPECT detects the substantial loss of dopamin-  
587 ergic neurons, markers based on this imaging modalities could be better  
588 employed in later stages of the disease, for example when motor symptoms  
589 appear.

590 Our work emphasizes the possibility to conveniently use complex network  
591 measures as PD markers. We demonstrated that, besides the high accuracy,  
592 MRI features based on complex networks bring a significant improvement to  
593 classification based only on clinical features. Classification is balanced, in  
594 fact specificity and sensitivity give similar results, unlike what we observed  
595 with clinical features which tend to be more specific but less sensitive. This

596 can be expected as the subjects included in this study are all considered at  
597 the baseline when the clinical symptoms are still mild.

598 Previous studies have usually investigated PD patterns basing on a re-  
599 stricted list of regions of interest (Braak et al., 2003; Burke et al., 2008).  
600 The reasons for such a choice are twofold: firstly, from a clinical perspective  
601 it is known that some regions are affected by the disease only at its later  
602 stages, as a consequence these regions can be safely disregarded; secondly,  
603 whole brain analysis can be too computationally intensive and when data  
604 samples are small it is easy to lack the statistical power required to detect  
605 small effects.

606 On the other hand, focusing on some regions can prevent the detection of  
607 interesting effects in the brain regions excluded or decrease the discrimination  
608 power of the approach. For example, (Worker et al., 2014) found no signif-  
609 icant cortical changes between PD patients and controls when examining a  
610 restricted list of brain regions.

611 It is worth noting that ROI-based approaches are intrinsically biased by  
612 segmentation errors which can prevent the methodologies to reach optimal  
613 sensitivity. This is why, even if using an ROI approach, we preferred a whole  
614 brain description. Our complex network approach significantly reduced the  
615 computational burden yielded by voxel-based approaches even if the number  
616 of examined regions was higher than in ROI-based studies.

617 In addition, our method is more sensitive than a standard VBM; as re-  
618 ported in previous studies, see for example (Focke et al., 2011), with VBM we  
619 observed no significant changes in cortical morphology when comparing NC  
620 and PD subjects. On the other hand the regions outlined with the proposed  
621 methodology are consistent with previous studies. Temporal and Frontal  
622 Gyri changes have shown atrophic patterns, especially in patients with de-  
623 mentia (Burton et al., 2004; Xia et al., 2013); cognitive impairment seems  
624 to acquire a relevant role for diagnosis also because of the inclusion of Brod-  
625 mann areas 24, 37, 44 and 46 as shown also in (Burton et al., 2004; Hughes  
626 et al., 1992; Nagano-Saito et al., 2005). As expected, Substantia Nigra and  
627 brain midstem also play a relevant role for the diagnosis. We found that  
628 most of the significant regions are not adjacent, indeed there is no a priori  
629 reason why adjacent patches (which can often include distinct anatomical  
630 districts) should share the same informative content, as neurodegenerative  
631 diseases may have a diffuse effect that involves multiple voxels not necessarily  
632 belonging to the same anatomical region Burton et al. (2004).

633 Our results outline the important role of combining MRI and clinical

634 features for an accurate early diagnosis. In fact, besides the increment of  
635 the classification accuracy, it is manifest that the use of clinical features is  
636 biased towards the NC class. We demonstrated that classification scores  
637 based only on clinical features were poorly sensitive, with lots of PD patients  
638 misclassified as controls; this effect is reasonable as in the early phase of the  
639 disease clinical symptoms are mild. On the other hand this result outlines  
640 the importance of complex network markers to improve both sensitivity and  
641 specificity of the classification.

## 642 **6. Conclusions**

643 In this work, we have demonstrated how complex networks can profi-  
644 ciently be used to define a novel brain connectivity and consequently intro-  
645 duce accurate markers for PD. We evaluated the robustness and the accuracy  
646 of the proposed methodology with both a direct evaluation, involving the  
647 measure of classification metrics, and an indirect check, regarding the brain  
648 regions mostly affected by the disease. We validated our method on a mixed  
649 cohort of controls and patients from the PPMI dataset; the proposed method-  
650 ology compares well with other state-of-the-art approaches for what concerns  
651 NC/PD classification. In addition, [our method allowed an investigation of  
652 the brain regions related to the disease starting from a segmentation com-  
653 pletely unsupervised over the whole brain without the necessity to \*a priori\*  
654 focus on specific anatomical regions](#), a fundamental aspect when looking for  
655 novel markers. Our results confirm what has been found in other studies and  
656 outlines new interesting aspects, specifically: (i) our work demonstrates that  
657 MRI data, and in particular complex network measures, provide an efficient  
658 and accurate description of PD patterns; (ii) novel MRI markers combined  
659 with clinical scores typical of prodromal PD can be used for an accurate  
660 early diagnosis; this approach (iii) compares favorably with state-of-the-art  
661 methodologies basing on MRI data and (iv) compares well with methodolo-  
662 gies including other imaging modalities such as SPECT. In brief, our work  
663 shows that the connectivity of several brain regions is significantly related to  
664 PD. Thus, we hope this result will stimulate further investigations to better  
665 understand the disease and its mechanisms. These results also suggest the  
666 applicability of the methodology to support PD diagnosis in clinical practice  
667 and possibly other disease affecting brain connectivity. Further studies could  
668 investigate how to improve this methodology, for example using multi-modal  
669 imaging data. In addition, it would be interesting to provide a comprehen-

670 sive model for the regions outlined by our approach from a more specifically  
671 clinical perspective.

## 672 **Acknowledgments**

673 PPMI, a public-private partnership, is funded by the Michael J. Fox Foun-  
674 dation for Parkinson’s Research and other funding partners include AbbVie,  
675 Avid Radiopharmaceuticals, Biogen Idec, Bristol-Myers Squibb, Covance,  
676 GE Healthcare, Genentech, GlaxoSmithKline, Eli Lilly and Company, Lund-  
677 beck, Merck & Co., Meso Scale Discovery, Pfizer, Piramal, Hoffmann-La  
678 Roche, and UCB (Union ChimiqueBelge). All authors disclose any actual  
679 or potential conflicts of interest, including any financial, personal, or other  
680 relationships with other people or organizations that could inappropriately  
681 influence their work. All experiments were performed with the informed  
682 consent of each participant or caregiver in line with the Code of Ethics of  
683 the World Medical Association (Declaration of Helsinki). Local institutional  
684 ethics committees approved the study.

## 685 **References**

- 686 Adeli, E., Shi, F., An, L., Wee, C.-Y., Wu, G., Wang, T., Shen, D., 2016.  
687 Joint feature-sample selection and robust diagnosis of Parkinson’s disease  
688 from MRI data. *NeuroImage* 141, 206–219.
- 689 Adeli, E., Wu, G., Saghafi, B., An, L., Shi, F., Shen, D., 2017. Kernel-based  
690 Joint Feature Selection and Max-Margin Classification for Early Diagnosis  
691 of Parkinson’s Disease. *Scientific Reports* 7, 41069.
- 692 Amoroso, N., Bellotti, R., Diacono, D., La Rocca, M., Tangaro, S., 2017.  
693 Salient Networks: A Novel Application to Study Brain Connectivity. In:  
694 International Conference on Bioinformatics and Biomedical Engineering.  
695 Springer, pp. 444–453.
- 696 Antonini, A., Leenders, K. L., Vontobel, P., Maguire, R. P., Missimer, J.,  
697 Psylla, M., Günther, I., 1997. Complementary PET studies of striatal  
698 neuronal function in the differential diagnosis between multiple system  
699 atrophy and Parkinson’s disease. *Brain* 120 (12), 2187–2195.
- 700 Ashburner, J., Friston, K. J., 2000. Voxel-based morphometrythe methods.  
701 *Neuroimage* 11 (6), 805–821.

- 702 Beyer, M. K., Janvin, C. C., Larsen, J. P., Aarsland, D., 2007. A magnetic  
703 resonance imaging study of patients with Parkinson's disease with mild  
704 cognitive impairment and dementia using voxel-based morphometry. *Journal of Neurology, Neurosurgery & Psychiatry* 78 (3), 254–259.  
705
- 706 Bouwmans, A. E., Vlaar, A. M., Mess, W. H., Kessels, A., Weber, W. E.,  
707 2013. Specificity and sensitivity of transcranial sonography of the substan-  
708 tia nigra in the diagnosis of Parkinson's disease: prospective cohort study  
709 in 196 patients. *BMJ open* 3 (4), e002613.
- 710 Braak, H., Del Tredici, K., Rüb, U., de Vos, R. A., Steur, E. N. J., Braak, E.,  
711 2003. Staging of brain pathology related to sporadic Parkinson's disease.  
712 *Neurobiology of aging* 24 (2), 197–211.
- 713 Breiman, L., 1996. Bagging predictors. *Machine learning* 24 (2), 123–140.
- 714 Breiman, L., 2001. Random forests. *Machine learning* 45 (1), 5–32.
- 715 Bullmore, E., Sporns, O., 2009. Complex brain networks: graph theoretical  
716 analysis of structural and functional systems. *Nature Reviews Neuroscience*  
717 10 (3), 186–198.
- 718 Burke, R. E., Dauer, W. T., Vonsattel, J. P. G., 2008. A critical evaluation  
719 of the Braak staging scheme for Parkinson's disease. *Annals of neurology*  
720 64 (5), 485–491.
- 721 Burton, E. J., McKeith, I. G., Burn, D. J., Williams, E. D., O'Brien, J. T.,  
722 2004. Cerebral atrophy in Parkinson's disease with and without dementia:  
723 a comparison with Alzheimer's disease, dementia with Lewy bodies and  
724 controls. *Brain* 127 (4), 791–800.
- 725 Chagas, M. H. N., Tumas, V., Pena-Pereira, M. A., Machado-de Sousa, J. P.,  
726 dos Santos, A. C., Sanches, R. F., Hallak, J. E., Crippa, J. A. S., 2017.  
727 Neuroimaging of major depression in Parkinson's disease: Cortical thick-  
728 ness, cortical and subcortical volume, and spectroscopy findings. *Journal*  
729 *of Psychiatric Research* 90, 40–45.
- 730 Chaudhuri, K. R., Healy, D. G., Schapira, A. H., 2006. Non-motor symptoms  
731 of Parkinson's disease: diagnosis and management. *The Lancet Neurology*  
732 5 (3), 235–245.

- 733 Cherubini, A., Morelli, M., Nisticó, R., Salsone, M., Arabia, G., Vasta, R.,  
734 Augimeri, A., Caligiuri, M. E., Quattrone, A., 2014. Magnetic resonance  
735 support vector machine discriminates between Parkinson disease and pro-  
736 gressive supranuclear palsy. *Movement Disorders* 29 (2), 266–269.
- 737 Cortes, C., Vapnik, V., 1995. Support-vector networks. *Machine learning*  
738 20 (3), 273–297.
- 739 Daianu, M., Jahanshad, N., Villalon-Reina, J. E., Mendez, M. F., Bartzokis,  
740 G., Jimenez, E. E., Joshi, A., Barsuglia, J., Thompson, P. M., 2014. Rich  
741 club network analysis shows distinct patterns of disruption in frontotemporal  
742 dementia and Alzheimer’s disease. In: *Computational Diffusion MRI*.  
743 Springer, pp. 13–22.
- 744 Dalrymple-Alford, J., MacAskill, M., Nakas, C., Livingston, L., Graham,  
745 C., Crucian, G., Melzer, T., Kirwan, J., Keenan, R., Wells, S., et al.,  
746 2010. The MoCA well-suited screen for cognitive impairment in Parkinson  
747 disease. *Neurology* 75 (19), 1717–1725.
- 748 Díaz-Uriarte, R., De Andres, S. A., 2006. Gene selection and classification of  
749 microarray data using random forest. *BMC bioinformatics* 7 (1), 3.
- 750 Dorsey, E., Constantinescu, R., Thompson, J., Biglan, K., Holloway, R.,  
751 Kieburtz, K., Marshall, F., Ravina, B., Schifitto, G., Siderowf, A., et al.,  
752 2007. Projected number of people with Parkinson disease in the most pop-  
753 ular nations, 2005 through 2030. *Neurology* 68 (5), 384–386.
- 754 Duchesne, S., Rolland, Y., Vérin, M., 2009. Automated computer differential  
755 classification in Parkinsonian syndromes via pattern analysis on MRI.  
756 *Academic radiology* 16 (1), 61–70.
- 757 Fischl, B., 2012. Freesurfer. *Neuroimage* 62 (2), 774–781.
- 758 Focke, N. K., Helms, G., Scheewe, S., Pantel, P. M., Bachmann, C. G.,  
759 Dechent, P., Ebentheuer, J., Mohr, A., Paulus, W., Trenkwalder, C.,  
760 2011. Individual voxel-based subtype prediction can differentiate progres-  
761 sive supranuclear palsy from idiopathic Parkinson syndrome and healthy  
762 controls. *Human brain mapping* 32 (11), 1905–1915.
- 763 Friedman, J., Friedman, H., 1993. Fatigue in Parkinson’s disease. *Neurology*  
764 43 (10), 2016–2016.



- 765 Gagnon, J.-F., Bédard, M.-A., Fantini, M., Petit, D., Panisset, M., Rompre,  
766 S., Carrier, J., Montplaisir, J., 2002. REM sleep behavior disorder and  
767 REM sleep without atonia in Parkinson’s disease. *Neurology* 59 (4), 585–  
768 589.
- 769 Gibb, W., Lees, A., 1988. The relevance of the lewy body to the pathogenesis  
770 of idiopathic parkinson’s disease. *Journal of Neurology, Neurosurgery &  
771 Psychiatry* 51 (6), 745–752.
- 772 Goetz, C. G., Tilley, B. C., Shaftman, S. R., Stebbins, G. T., Fahn, S.,  
773 Martinez-Martin, P., Poewe, W., Sampaio, C., Stern, M. B., Dodel, R.,  
774 et al., 2008. Movement Disorder Society-sponsored revision of the Unified  
775 Parkinson’s Disease Rating Scale (MDS-UPDRS): Scale presentation and  
776 clinimetric testing results. *Movement disorders* 23 (15), 2129–2170.
- 777 Hansen, A. K., Knudsen, K., Lillethorup, T. P., Landau, A. M., Parbo, P.,  
778 Fedorova, T., Audrain, H., Bender, D., Østergaard, K., Brooks, D. J.,  
779 et al., 2016. In vivo imaging of neuromelanin in Parkinson’s disease using  
780 18F-AV-1451 PET. *Brain*, aww098.
- 781 Hirschauer, T. J., Adeli, H., Buford, J. A., 2015. Computer-aided diagnosis of  
782 Parkinson’s disease using enhanced probabilistic neural network. *Journal  
783 of medical systems* 39 (11), 179.
- 784 Hoehn, M. M., Yahr, M. D., et al., 1998. Parkinsonism: onset, progression,  
785 and mortality. *Neurology* 50 (2), 318–318.
- 786 Huber, S. J., Shuttlesworth, E. C., Paulson, G. W., 1986. Dementia in Parkin-  
787 son’s disease. *Archives of Neurology* 43 (10), 987–990.
- 788 Hughes, A. J., Daniel, S. E., Kilford, L., Lees, A. J., 1992. Accuracy of clinical  
789 diagnosis of idiopathic Parkinson’s disease: a clinico-pathological study of  
790 100 cases. *Journal of Neurology, Neurosurgery & Psychiatry* 55 (3), 181–  
791 184.
- 792 Jankovic, J., 2008. Parkinson’s disease: clinical features and diagnosis. *Jour-  
793 nal of Neurology, Neurosurgery & Psychiatry* 79 (4), 368–376.
- 794 Jenkinson, M., Bannister, P., Brady, M., Smith, S., 2002. Improved optimiza-  
795 tion for the robust and accurate linear registration and motion correction  
796 of brain images. *Neuroimage* 17 (2), 825–841.

- 797 Jenkinson, M., Smith, S., 2001. A global optimisation method for robust  
798 affine registration of brain images. *Medical image analysis* 5 (2), 143–156.
- 799 Johns, M. W., et al., 1991. A new method for measuring daytime sleepiness:  
800 the Epworth sleepiness scale. *sleep* 14 (6), 540–545.
- 801 Kalia, L. V., Lang, A. E., April 2015. Parkinson’s disease. *Lancet* 386 (9996),  
802 896–912.
- 803 Kim, H. J., Kim, S. J., Kim, H. S., Choi, C. G., Kim, N., Han, S., Jang, E. H.,  
804 Chung, S. J., Lee, C. S., 2013. Alterations of mean diffusivity in brain white  
805 matter and deep gray matter in parkinson’s disease. *Neuroscience letters*  
806 550, 64–68.
- 807 Kwon, D.-H., Kim, J.-M., Oh, S.-H., Jeong, H.-J., Park, S.-Y., Oh, E.-S.,  
808 Chi, J.-G., Kim, Y.-B., Jeon, B. S., Cho, Z.-H., 2012. Seven-tesla magnetic  
809 resonance images of the substantia nigra in Parkinson disease. *Annals of*  
810 *neurology* 71 (2), 267–277.
- 811 La Rocca, M., Amoroso, N., Bellotti, R., Diacono, D., Monaco, A., Monda,  
812 A., Tateo, A., Tangaro, S., 2017. A Multiplex Network Model to Charac-  
813 terize Brain Atrophy in Structural MRI. In: *Emergent Complexity from*  
814 *Nonlinearity, in Physics, Engineering and the Life Sciences*. Springer, pp.  
815 189–198.
- 816 Li, X., Xing, Y., Schwarz, S. T., Auer, D. P., 2017. Limbic grey matter  
817 changes in early parkinson’s disease. *Human Brain Mapping*.
- 818 Litvan, I., Goldman, J. G., Tröster, A. I., Schmand, B. A., Weintraub, D.,  
819 Petersen, R. C., Mollenhauer, B., Adler, C. H., Marder, K., Williams-  
820 Gray, C. H., et al., 2012. Diagnostic criteria for mild cognitive impairment  
821 in Parkinson’s disease: Movement Disorder Society Task Force guidelines.  
822 *Movement Disorders* 27 (3), 349–356.
- 823 Lo, C.-Y., Wang, P.-N., Chou, K.-H., Wang, J., He, Y., Lin, C.-P., 2010.  
824 Diffusion tensor tractography reveals abnormal topological organization in  
825 structural cortical networks in Alzheimer’s disease. *Journal of Neuroscience*  
826 30 (50), 16876–16885.
- 827 Marek, K., Jennings, D., Lasch, S., Siderowf, A., Tanner, C., Simuni, T., Cof-  
828 fey, C., Kieburtz, K., Flagg, E., Chowdhury, S., et al., 2011. The parkinson

- 829 progression marker initiative PPMI. *Progress in neurobiology* 95 (4), 629–  
830 635.
- 831 Marquand, A. F., Filippone, M., Ashburner, J., Girolami, M., Mourao-  
832 Miranda, J., Barker, G. J., Williams, S. C., Leigh, P. N., Blain, C. R.,  
833 2013. Automated, high accuracy classification of parkinsonian disorders: a  
834 pattern recognition approach. *PloS one* 8 (7), e69237.
- 835 Masdeu, J. C., 2017. Future Directions in Imaging Neurodegeneration. *Cur-  
836 rent Neurology and Neuroscience Reports* 17 (1), 9.
- 837 Menichetti, G., Remondini, D., Panzarasa, P., Mondragón, R. J., Bianconi,  
838 G., 2014. Weighted multiplex networks. *PloS one* 9 (6), e97857.
- 839 Miller, D. B., O’Callaghan, J. P., 2015. Biomarkers of Parkinson’s disease:  
840 present and future. *Metabolism* 64 (3), S40–S46.
- 841 Nagano-Saito, A., Washimi, Y., Arahata, Y., Kachi, T., Lerch, J., Evans, A.,  
842 Dagher, A., Ito, K., 2005. Cerebral atrophy and its relation to cognitive  
843 impairment in Parkinson disease. *Neurology* 64 (2), 224–229.
- 844 Pilotto, A., Yilmaz, R., Berg, D., 2015. Developments in the role of tran-  
845 scranial sonography for the differential diagnosis of parkinsonism. *Current  
846 neurology and neuroscience reports* 15 (7), 1–10.
- 847 Postuma, R. B., Aarsland, D., Barone, P., Burn, D. J., Hawkes, C. H., Oertel,  
848 W., Ziemssen, T., 2012. Identifying prodromal Parkinson’s disease: Pre-  
849 Motor disorders in Parkinson’s disease. *Movement Disorders* 27 (5), 617–  
850 626.
- 851 Postuma, R. B., Berg, D., Stern, M., Poewe, W., Olanow, C. W., Oertel, W.,  
852 Obeso, J., Marek, K., Litvan, I., Lang, A. E., et al., 2015. MDS clinical  
853 diagnostic criteria for Parkinson’s disease. *Movement Disorders* 30 (12),  
854 1591–1601.
- 855 Saeys, Y., Inza, I., Larrañaga, P., 2007. A review of feature selection tech-  
856 niques in bioinformatics. *bioinformatics* 23 (19), 2507–2517.
- 857 Salvatore, C., Cerasa, A., Castiglioni, I., Gallivanone, F., Augimeri, A.,  
858 Lopez, M., Arabia, G., Morelli, M., Gilardi, M., Quattrone, A., 2014.

- 859 Machine learning on brain MRI data for differential diagnosis of Parkin-  
860 son's disease and Progressive Supranuclear Palsy. *Journal of Neuroscience*  
861 *Methods* 222, 230–237.
- 862 Singaram, C., Gaumnitz, E., Torbey, C., Ashraf, W., Quigley, E., Sen-  
863 gupta, A., Pfeiffer, R., 1995. Dopaminergic defect of enteric nervous sys-  
864 tem in Parkinson's disease patients with chronic constipation. *The Lancet*  
865 346 (8979), 861–864.
- 866 Singh, G., Samavedham, L., 2015. Unsupervised learning based feature ex-  
867 traction for differential diagnosis of neurodegenerative diseases: a case  
868 study on early-stage diagnosis of Parkinson disease. *Journal of neuroscience*  
869 *methods* 256, 30–40.
- 870 Smith, S. M., 2002. Fast robust automated brain extraction. *Human brain*  
871 *mapping* 17 (3), 143–155.
- 872 Stam, C., Jones, B., Nolte, G., Breakspear, M., Scheltens, P., 2007. Small-  
873 world networks and functional connectivity in Alzheimer's disease. *Cere-*  
874 *bral cortex* 17 (1), 92–99.
- 875 Stiasny-Kolster, K., Mayer, G., Schäfer, S., Möller, J. C., Heindel-  
876 Gutenbrunner, M., Oertel, W. H., 2007. The REM sleep behavior disorder  
877 screening questionnaire: a new diagnostic instrument. *Movement disorders*  
878 22 (16), 2386–2393.
- 879 Summerfield, C., Junqué, C., Tolosa, E., Salgado-Pineda, P., Gómez-Ansón,  
880 B., Martí, M. J., Pastor, P., Ramírez-Ruíz, B., Mercader, J., 2005. Struc-  
881 tural brain changes in Parkinson disease with dementia: a voxel-based  
882 morphometry study. *Archives of Neurology* 62 (2), 281–285.
- 883 Suwijn, S. R., van Boheemen, C. J., de Haan, R. J., Tissingh, G., Booij,  
884 J., de Bie, R. M., 2015. The diagnostic accuracy of dopamine transporter  
885 SPECT imaging to detect nigrostriatal cell loss in patients with Parkin-  
886 son's disease or clinically uncertain parkinsonism: a systematic review.  
887 *EJNMMI research* 5 (1), 12.
- 888 Tessa, C., Lucetti, C., Giannelli, M., Diciotti, S., Poletti, M., Danti, S.,  
889 Baldacci, F., Vignali, C., Bonuccelli, U., Mascalchi, M., et al., 2014. Pro-  
890 gression of brain atrophy in the early stages of Parkinson's disease: A

- 891 longitudinal tensor-based morphometry study in de novo patients without  
892 cognitive impairment. *Human brain mapping* 35 (8), 3932–3944.
- 893 Tijms, B. M., Wink, A. M., de Haan, W., van der Flier, W. M., Stam, C. J.,  
894 Scheltens, P., Barkhof, F., 2013. Alzheimer’s disease: connecting findings  
895 from graph theoretical studies of brain networks. *Neurobiology of aging*  
896 34 (8), 2023–2036.
- 897 Warmuth-Metz, M., Naumann, M., Csoti, I., Solymosi, L., 2001. Measure-  
898 ment of the midbrain diameter on routine magnetic resonance imaging: a  
899 simple and accurate method of differentiating between parkinson disease  
900 and progressive supranuclear palsy. *Archives of neurology* 58 (7), 1076–  
901 1079.
- 902 Wen, M.-C., Ng, A., Chander, R. J., Au, W. L., Tan, L. C., Kandiah, N.,  
903 2015. Longitudinal brain volumetric changes and their predictive effects  
904 on cognition among cognitively asymptomatic patients with parkinson’s  
905 disease. *Parkinsonism & related disorders* 21 (5), 483–488.
- 906 Worker, A., Blain, C., Jarosz, J., Chaudhuri, K. R., Barker, G. J., Williams,  
907 S. C., Brown, R., Leigh, P. N., Simmons, A., 2014. Cortical thickness,  
908 surface area and volume measures in Parkinson’s disease, multiple system  
909 atrophy and progressive supranuclear palsy. *PloS one* 9 (12), e114167.
- 910 Xia, J., Miu, J., Ding, H., Wang, X., Chen, H., Wang, J., Wu, J., Zhao, J.,  
911 Huang, H., Tian, W., et al., 2013. Changes of brain gray matter structure  
912 in Parkinson’s disease patients with dementia. *Neural regeneration research*  
913 8 (14), 1276.
- 914 Yesavage, J., Brink, T., Rose, T., et al., 2000. Geriatric depression scale  
915 (GDS). *Handbook of psychiatric measures*. Washington DC: American  
916 Psychiatric Association, 544–6.
- 917 Yesavage, J. A., Sheikh, J. I., 1986. 9/Geriatric depression scale (GDS) recent  
918 evidence and development of a shorter version. *Clinical gerontologist* 5 (1-  
919 2), 165–173.